Attosecond Lighthouses: How To Use Spatiotemporally Coupled Light Fields To Generate Isolated Attosecond Pulses

Fabien Quéré, H. Vincenti

Attosecond Lighthouses: How To Use Spatiotemporally Coupled Light Fields To Generate Isolated Attosecond Pulses

H. Vincenti and F. Quéré*

CEA, IRAMIS, Service des Photons Atomes et Molécules, F-91191 Gif-sur-Yvette, France

(Received 23 September 2011; published 16 March 2012)

Under the effect of even simple optical components, the spatial properties of femtosecond laser beams can vary over the duration of the light pulse. We show how using such spatiotemporally coupled light fields in high harmonic generation experiments (e.g., in gases or dense plasmas) enables the production of attosecond lighthouses, i.e., sources emitting a collection of angularly well-separated light beams, each consisting of an isolated attosecond pulse. This general effect opens the way to a new generation of light sources, particularly suitable for attosecond pump-probe experiments, and provides a new tool for ultrafast metrology, for instance, giving direct access to fluctuations of the carrier-envelope relative phase of even the most intense ultrashort lasers.

DOI: 10.1103/PhysRevLett.108.113904 PACS numbers: 42.65.Ky, 42.65.Re

Ultrashort light beams are said to exhibit spatiotemporal couplings (STCs) when their spatial properties depend on time, and conversely [1]—i.e., their electric field $E(x, y, z = z_0, t) \neq E_1(t)E_2(x, y)$. The importance of STCs has been largely overlooked in most laser-matter interaction experiments, until recently [2]. In strong-field science, STCs are even considered as highly detrimental, because they systematically decrease the peak intensity at focus [3]. In this Letter, we show that, on the opposite, moderate and controlled STCs provide a powerful means of controlling high-intensity laser-matter interactions and pave the way to a whole range of new experimental capabilities.

To demonstrate this idea, we consider a particular application of STCs to the generation of isolated attosecond (1 as $= 10^{-18}$ s) pulses, which has been the key issue in the development of attosecond science [4]. All attosecond light sources demonstrated so far are based on high-order harmonic generation (HHG) with intense femtosecond laser pulses in different media [4,5]. Since many-cycle long pulses naturally produce trains of attosecond pulses, considerable efforts had to be deployed in the past 15 years for the development of ''temporal gating'' techniques, to isolate single attosecond pulses, more readily usable for time-resolved measurements of electron dynamics in matter. For HHG in gases, several techniques have now been demonstrated [6–8], but they remain experimentally challenging. Moreover, despite a few theoretical proposals [9–11], this problem is still unsolved experimentally for HHG on plasma mirrors, one of the promising processes to obtain the next generation of attosecond light sources [12,13].

We describe here a new approach to this problem, of unprecedented simplicity, generality, and potential: One of the most basic types of STCs, wave-front rotation [1] (WFR), can be exploited to generate a collection of single attosecond pulses in angularly well-separated light beams—an attosecond lighthouse—even with relatively long laser pulses. In contrast to the specific interaction scheme proposed in Ref. [11] to achieve such an angular separation, the method described here is general and produces beams in well-controlled directions.

Let us first briefly summarize the concept of WFR at the focus of a femtosecond laser beam [14]. Out of focus, this STC takes a different form, called pulse-front tilt, which corresponds to an E field of the form (assuming Gaussian profiles in time and space)

$$E(x_i, t) = E_0 \exp\left(-2\left[\frac{t - \xi x_i}{\tau_i}\right]^2 - 2\frac{x_i^2}{w_i^2} + i\omega_L t\right), \quad (1)$$

where x_i is one of the transverse spatial coordinates, τ_i the Fourier-transform limited pulse duration at a given position in the beam, w_i the beam diameter before focusing, ξ the pulse-front tilt parameter, and ω_L the laser central frequency. All widths are defined as full widths at $1/e$ of the intensity profile. Pulse-front tilt occurs whenever $\xi \neq 0$, i.e., when the line formed by the pulse maxima in the (x_i, t) space—the pulse front—is tilted with respect to the wave fronts [see Figs. 1(a) and 1(b)].

For instance, pulse-front tilt can be induced upon diffraction on a grating: Since the incidence angle α_i and diffraction angle α_d are not equal [Fig. 1(a)], the accumulated optical path length varies with transverse coordinate x_i, resulting in a varying delay between the wave front and pulse front across the beam. In chirped-pulse amplification lasers, residual pulse-front tilt thus occurs whenever some of the gratings used in the compressor are not exactly parallel [see Fig. 1(a)].

This example provides a straightforward way of understanding the E-field configuration once a beam with initial pulse-front tilt is focused. Indeed, a grating followed by a focusing element acts as spectrometer. At focus, such a beam thus presents a spectrum which depends on space [15], as illustrated in Fig. 1(c). This effect is known as

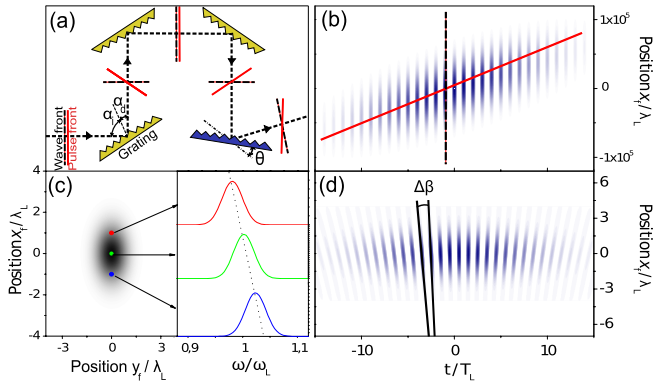

FIG. 1 (color online). Pulse-front tilt and wave-front rotation of a femtosecond laser beam. Panel (a) illustrates how a slightly misaligned four-grating compressor leads to a residual pulse-front tilt at its output. (b) E field before focusing [real part of Eq. (1)], exhibiting pulse-front tilt. Blue corresponds to $E \geq 0$ and white to $E < 0$. (c) 2D-intensity distribution and spectrum at focus. The focal spot is elongated, and the field spectrum varies spatially along the long direction of the ellipse. (d) Associated E field at focus [real part of Eq. (2)], exhibiting wave-front rotation in time. Laser pulse parameters are $\tau_i = 25$ fs, $w_i = 70$ mm, and $\xi = \tau_i/w_i = 0.36$ fs/mm. With $f = 200$ mm, this leads to $w_f = 2.6\lambda_L$, $\tau_f = 35$ fs, and $v_r = 7$ mrad/fs. These parameters are typical of a state-of-the-art high-power femtosecond laser.

spatial chirp in the (x_f, ω) space, where x_f is the transverse spatial coordinate at focus and ω the light frequency. As ξ increases, the focal spot becomes more and more elliptical, with a long axis along the direction of spatial chirp [see Fig. 1(c)].

In the (x_f, t) domain, such a spatial chirp implies that the time spacing between successive wave fronts varies with the transverse coordinate x_f: As a result, the wave fronts rotate in time [see Fig. 1(d)]. Indeed, calculating the Fourier transform $\tilde{E}(k, t)$ of $E(x_i, t)$ with respect to x_i and using $k = k_L x_f/f$ (where $k_L = \omega_L/c = 2\pi/\lambda_L$ is the laser wave vector) leads to the field $\tilde{E}(x_f, t)$ at the focus of an optics of focal length f:

$$\tilde{E}(x_f, t) \propto \exp\left(-2\frac{t^2}{\tau_f^2} - 2\frac{x_f^2}{w_f^2}\right)\exp[i\varphi(x_f, t)],$$
$$\varphi(x_f, t) = 4\frac{w_i\xi}{w_f\tau_f\tau_i}x_f t + \omega_L t, \tag{2}$$

where the pulse duration τ_f at focus and the effective beam waist w_f along the x_f axis are given by

$$\tau_f/\tau_i = w_f/w_0 = \sqrt{1 + (w_i\xi/\tau_i)^2} \tag{3}$$

with $w_0 = 2(\lambda_L f/\pi w_i)$ the usual beam waist at focus when $\xi = 0$. The instantaneous direction of propagation of light $\beta(t)$ is given by $\beta \approx k_\perp(t)/k_L$, where $k_L = \omega_L/c$ is the laser wave vector and $k_\perp(t) = \partial\varphi/\partial x_f$ its transverse component. The $x_f t$ term in φ implies that β, and hence the instantaneous wave-front direction, vary in time, with a rotation velocity $v_r = d\beta/dt$ deduced from Eq. (2):

$$v_r = \frac{w_i^2}{f\tau_i^2}\frac{\xi}{1 + (w_i\xi/\tau_i)^2}. \tag{4}$$

For given duration τ_i and divergence $\theta_L = w_i/f$ of the beam, $v_r(\xi)$ has a maximum allowed value of $v_r^{\max} = w_i/2f\tau_i = \theta_L/2\tau_i$, achieved for $\xi_0 = \tau_i/w_i$. Intuitively, this is because $v_r \approx \Delta\theta/\Delta T$, where $\Delta\theta$ is the angle that is streaked by the field wave vector and ΔT is the time required for this streaking. The maximum in v_r is thus achieved when light roughly sweeps the largest possible angle ($\Delta\theta \approx \theta_L$), in the shortest achievable duration for this pulse ($\Delta T \approx \tau_i$). This optimum case corresponds to a pulse-front delay of τ_i across the laser beam diameter w_i before focusing, while at focus $w_f = \sqrt{2}w_0$ and $\tau_f = \sqrt{2}\tau_i$, leading to a reduction of the peak intensity by a factor of 2 only compared to the case when $\xi = 0$. For a 25 fs laser pulse focused with $\theta_L = 0.35$ rad ($w_i \approx f/3$), $v_r^{\max}$ reaches the considerable value of 7 mrad/fs, i.e., $\approx 10^{12}$ revolutions per second.

WFR has an immediate and far-reaching interest in the context of attosecond pulse generation. When a usual laser pulse is used to drive HHG in gases or plasmas, the generated train of N attosecond pulses is generally produced within a collimated beam, with a divergence smaller than that of the initial laser beam. In contrast, in the presence of WFR, due to the coherence of HHG, these N attosecond pulses are all emitted in slightly different directions, which correspond to the instantaneous directions of propagation of the laser field at the times of generation.

This attosecond lighthouse effect can be exploited to produce N angularly well-separated short-wavelength beams, each one containing a single attosecond pulse. To achieve such a result, the rotation $\Delta\beta = v_r\Delta t$ of the wave front in the time interval Δt between the emissions of two successive attosecond pulses has to be larger than the divergence θ_n of the short-wavelength light beam around frequency $n\omega_L$. Since for given laser beam parameters, $\Delta\beta$ cannot exceed $v_r^{\max}\Delta t = \theta_L\Delta t/2\tau_i$, this is possible only provided the divergence of the harmonic beam is small enough, i.e.,

$$\frac{\theta_n}{\theta_L} \leq \frac{1}{\alpha p N_c}, \tag{5}$$

where $N_c \geq N$ is the number of optical cycles in the driving-laser pulse, p the number of attosecond pulses generated every laser optical cycle, and $\alpha = O(1)$ a prefactor which depends on the intensity contrast required between a given attosecond pulse and its first satellites [15]. Equation (5) determines the duration of the longest laser pulses that can be used to drive an attosecond lighthouse, for a given ratio of harmonic and laser divergence—which is generally imposed by the physics

of the generation process and the experimental configuration.

Since the attosecond lighthouse effect does not rely on a specific property of a given physical process, it in principle applies to any HHG mechanism, in particular, HHG through electron-ion recollision in gases. Its implementation requires only a slight rotation of one of the gratings in the compressor of a chirped-pulse amplification laser or introducing an adequate prism in the beam [15]. This extreme simplicity of implementation is particularly appreciable in the case of plasma mirrors, which require very high-power lasers, for which the gating techniques studied theoretically so far [9–11] are in practice very challenging to apply.

In this perspective, we now focus on the particular case of HHG on plasma mirrors in the relativistic interaction regime, in order to validate the basic effects previously described. As an intense laser field reflects on a dense plasma with a sharp surface, it induces an oscillation of the plasma surface, which generates through the Doppler effect high-order harmonics in the reflected beam, associated to trains of attosecond pulses.

We first describe this process with the simple relativistic oscillating mirror (ROM) model described in Ref. [16], which we use to calculate the reflected E field, in the presence of WFR. In this model, the position $Z(x_f, t)$ of the plasma surface at the transverse position x_f follows an harmonic oscillation at the laser frequency, with peak velocity $v_m/c = a/\sqrt{1+a^2}$, where $a(x_f, t)$ is the spatio-temporal envelope of the normalized vector potential of the incident laser. This leads to $Z(x_f, t) = (v_m/\omega_L) \times \cos\varphi(x_f, t)$, with φ given by Eq. (2). The reflected field $\tilde{E}_r(x_f, t)$ is then proportional to $\tilde{E}(x_f, t_{\mathrm{ret}})e^{ik_L Z(t_{\mathrm{ret}})}$, where $t_{\mathrm{ret}}(x_f)$ is the solution of $Z(x_f, t_{\mathrm{ret}}) = c(t - t_{\mathrm{ret}})$. This accounts for retardation effects in light propagation and, hence, for the Doppler effect induced by the plasma mirror surface oscillations. Once the reflected field $\tilde{E}_r(x_f, z = 0, t)$ right after the target is obtained, we calculate its propagation in vacuum by using plane waves decomposition in order to determine its structure $E_r(x, z, t)$ at arbitrary distance z from the target.

The predictions of this model are displayed in Fig. 2, for different WFR velocities, from 0 to $v_r^{\max}$. As expected, in the absence of WFR, harmonics of the laser frequency are emitted in a single collimated beam [Fig. 2(a)], with a divergence weaker than that of the fundamental frequency, and are associated in the time domain to a train of 5 attosecond pulses [Fig. 2(b)]. As v_r increases, this single beam progressively splits into a set of different beams [Figs. 2(c) and 2(e)]. At the optimum rotation velocity, these beams are angularly well-separated [Fig. 2(e)]; each of them carries a continuous electromagnetic spectrum and is associated to a single attosecond pulse [Fig. 2(f)].

To confirm the predictions of this simple model, we have performed 2D particle-in-cell (PIC) simulations of HHG

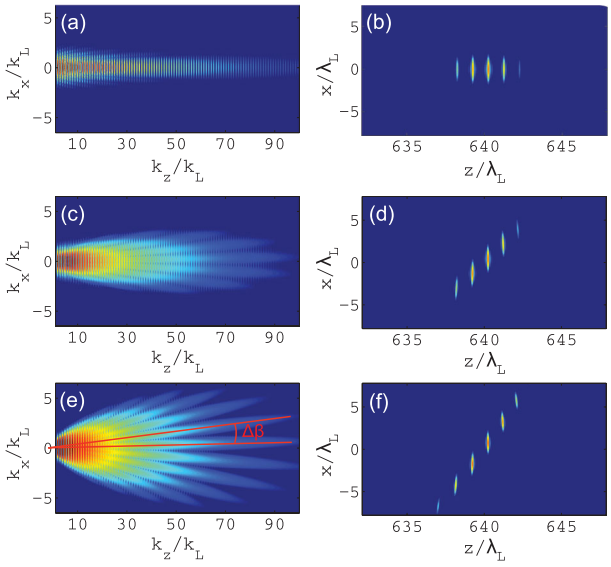

FIG. 2 (color). Results of the ROM model for the attosecond lighthouse effect. The parameters of the laser beam are the same as in Fig. 1, and the normalized vector potential $a_0 = 3$. The top row corresponds to $\xi = 0$, the middle one to $\xi = \tau_i/2w_i$, and the bottom one to $\xi = \tau_i/w_i$ (maximum rotation velocity). The left panels show the 2D Fourier transform of the field $\tilde{E}(x_f, t)$ after the HHG interaction. In these plots, the distance from origin corresponds to frequency, and the polar angle corresponds to the propagation direction. The right panels show instantaneous snapshots of the intensity of the attosecond pulses corresponding to harmonic orders 70–80, as a function of transverse and longitudinal spatial coordinates x and z, at a distance from the source larger than the Rayleigh length of the corresponding harmonics.

on plasma mirrors, in the ROM regime [13] ($a_0 = 6$), including WFR, using the CALDER code. In the case presented in Fig. 3, the plasma has a maximum density of $100n_c$, an initial density gradient of $\lambda_L/200$, and an initial electronic temperature of 0.1 keV, and ions are mobile. The incidence angle is 45°, and the laser field is p-polarized. This field is injected in the simulation box through boundary conditions, in the form of Eq. (2). The field $\tilde{E}_r(x_f, t)$ right after the target, obtained by PIC simulations, is propagated over arbitrary distances by using again plane waves decomposition. With the rotation velocity set at its maximum value, the attosecond lighthouse effect is clearly observed [see Fig. 3(a) and the movie in Ref. [15]]. This rotation velocity is large enough, and the short-wavelength light beam divergence small enough, to isolate a single attosecond pulse by simply setting a slit in the far field [Fig. 3(b)]. This shows that fulfilling Eq. (5) is physically realistic for plasma mirrors.

We finally discuss the various applications of the attosecond lighthouse effect. As far as the generation of isolated attosecond pulses is concerned, this effect provides an ideal optical scheme for attosecond pump-probe experiments, which avoids critical temporal jitter issues related to the use of multiple laser pulses. Indeed, two or more

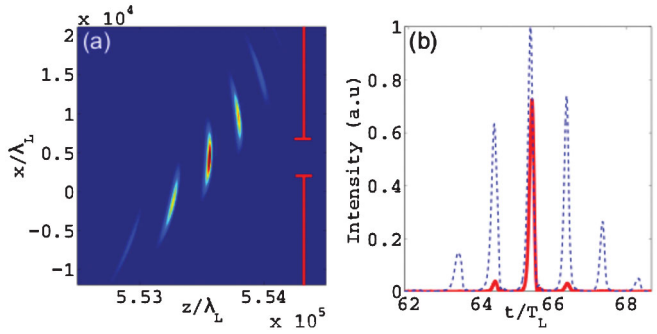

FIG. 3 (color). Particle-in-cell simulation of the attosecond lighthouse effect. The left panel shows the far-field intensity distribution of the attosecond pulses (harmonic orders 15–30) generated when an intense laser field ($a_0 = 6$, $w_f = 8\lambda_L$, $\tau_f =$ 22 fs, $\theta_L = 56$ mrad), with a WFR velocity $v_r = v_r^{\max} =$ 1.3 mrad/fs, reflects on a plasma mirror where it induces the ROM effect. These physical parameters are experimentally realistic, and the obtained ratio of harmonic and laser divergences consistent with experimental data [23]. The right panel shows the angularly integrated temporal intensity profile of this field (red curve), after filtering by the diaphragm displayed in red in the left panel, which selects $\approx 60\%$ of the main pulse energy. The blue curve corresponds to the temporal profile obtained from a PIC simulation in the same interaction conditions, but without WFR. Both curves have been normalized by the peak intensity of the train without WFR.

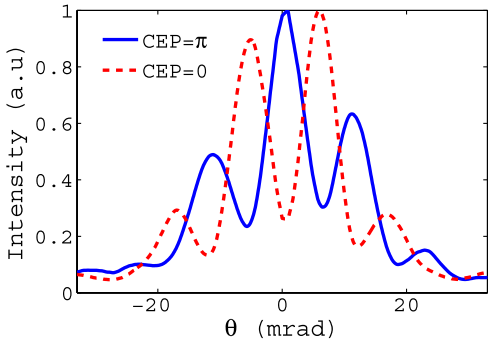

FIG. 4 (color online). Sensitivity to the carrier-envelope relative phase of the driving laser. The curves display the spatial profile of the spectrally integrated harmonic signal (from orders 25–30) in the far field, for two values of the driving-laser pulse CEP differing by π, obtained from PIC simulations, for the same physical parameters as in Fig. 3.

perfectly synchronized single attosecond pulses can be generated *with a single laser pulse*, in spatially separated beams, by setting adequate spatial masks in the far field. These multiple pulses can then be manipulated with a few independent optics and recombined with a variable delay on a target.

This effect also has great potential in terms of metrology. It indeed provides a direct way of studying the properties of all individual attosecond pulses generated along a laser pulse. The propagation directions of the N attosecond pulses are directly related to their times of emission, and by measurements on the different beams, the spectrum, divergence, and relative energy of each of these pulses can be determined. This not only provides direct information on the physics of the generation process but will also be particularly useful in experiments that exploit HHG as a probe of the generating medium, since it constitutes a stroboscope, that can, for instance, register the temporal evolution of molecular orbitals [17,18] with attosecond resolution over the whole laser pulse duration, without the need to scan any delay.

Last, since the emission times of the attosecond pulses depend linearly on the carrier-envelope relative phase (CEP) [19] of the driving-laser pulse, changes in the CEP result in shifts of the emission angular pattern under the beam spatial envelope, as illustrated in Fig. 4. On the one hand, this implies that CEP stabilization is still required to achieve shot-to-shot reproducibility of this source. But, on the other hand, when CEP is not stabilized, measuring the harmonic beam angular pattern provides a straightforward means of tracking CEP variations right at focus and of binning any experimental data obtained on different laser shots as a function of its actual value. In combination with the use of plasma mirrors for HHG, this opens the way to CEP-resolved experiments in the relativistic interaction regime.

In conclusion, wave-front rotation constitutes a very powerful tool for attosecond science and provides an ideal scheme to isolate highly collimated attosecond pulses in the x-ray range from beams reflected on plasma mirrors [20–22]. More generally, while spatiotemporal couplings of ultrafast laser beams have so far mostly been considered as detrimental, this Letter illustrates how shaping light fields in both time and space can provide new degrees of freedom to manipulate matter with intense light, leading to new experimental capabilities.

The research leading to these results has received funding from the European Research Council (ERC Grant Agreement No. 240013) and Laserlab-ALADIN (Grant No. 228334). This work was performed by using HPC resources from GENCI-CCRT/CINES (Grant No. 2011-056057). The authors gratefully acknowledge E. Lefebvre for providing the PIC code CALDER, R. Nuter for modifying this code to include WFR, and useful discussions with O. Gobert, M. Comte, and G. Bonnaud.

*Corresponding author.
fabien.quere@cea.fr

[1] S. Akturk, X. Gu, P. Bowlan, and R. Trebino, J. Opt. **12**, 093001 (2010).
[2] D. Vitek, E. Block, Y. Bellouard, and D. Adams, Opt. Express **18**, 24 673 (2010).
[3] G. Pretzler, A. Kasper, and K. J. Witte, Appl. Phys. B **70**, 1 (2000).
[4] F. Krausz and M. Ivanov, Rev. Mod. Phys. **81**, 163 (2009).

[5] Y. Nomura *et al.*, Nature Phys. **5**, 124 (2008).
[6] G. Sansone *et al.*, Science **314**, 443 (2006).
[7] E. Goulielmakis *et al.*, Science **320**, 1614 (2008).
[8] X. Feng *et al.*, Phys. Rev. Lett. **103**, 183901 (2009).
[9] G. D. Tsakiris, K. Eidmann, J. Meyer-ter-Vehn, and F. Krausz, New J. Phys. **8**, 19 (2006).
[10] T. Baeva, S. Gordienko, and A. Pukhov, Phys. Rev. E **74**, 065401 (2006).
[11] N. M. Naumova, J. A. Nees, I. V. Sokolov, B. Hou, and G. A. Mourou, Phys. Rev. Lett. **92**, 063902 (2004).
[12] U. Teubner and P. Gibbon, Rev. Mod. Phys. **81**, 445 (2009).
[13] C. Thaury and F. Quéré, J. Phys. B **43**, 213001 (2010).
[14] S. Akturk, X. Gu, P. Gabolde, and R. Trebino, Opt. Express **13**, 8642 (2005).
[15] See Supplemental Material at http://link.aps.org/supplemental/10.1103/PhysRevLett.108.113904 for supplementary information.
[16] R. Lichters, J. Meyer-ter-Vehn, and A. Pukhov, Phys. Plasmas **3**, 3425 (1996).
[17] J. Itatani *et al.*, Nature (London) **432**, 867 (2004).
[18] H. J. Wörner, J. B. Bertrand, D. V. Kartashov, P. B. Corkum, and D. M. Villeneuve, Nature (London) **466**, 604 (2010).
[19] S. T. Cundiff and Jun Ye, Rev. Mod. Phys. **75**, 325 (2003).
[20] S. Gordienko, A. Pukhov, O. Shorokhov, and T. Baeva, Phys. Rev. Lett. **93**, 115002 (2004).
[21] B. Dromey *et al.*, Nature Phys. **2**, 456 (2006).
[22] B. Dromey *et al.*, Phys. Rev. Lett. **99**, 085001 (2007).
[23] B. Dromey *et al.*, Nature Phys. **5**, 146 (2009).